Resource efficient plasmon-based 2D-photovoltaics with reflective support

Carl Hägglund* **and S. Peter Apell**

Department of Applied Physics, Chalmers University of Technology
SE-412 96 Göteborg, Sweden
**carl.hagglund@chalmers.se*

Abstract: For ultrathin (~10 nm) nanocomposite films of plasmonic materials and semiconductors, the absorptance of normal incident light is typically limited to about 50%. However, through addition of a non-absorbing spacer with a highly reflective backside to such films, close to 100% absorptance can be achieved at a targeted wavelength. Here, a simple analytic model useful in the long wavelength limit is presented. It shows that the spectral response can largely be characterized in terms of two wavelengths, associated with the absorber layer itself and the reflective support, respectively. These parameters influence both absorptance peak position and shape. The model is employed to optimize the system towards broadband solar energy conversion, with the spectrally integrated plasmon induced semiconductor absorptance as a figure of merit. Geometries optimized in this regard are then evaluated in full finite element calculations which demonstrate conversion efficiencies of up to 64% of the Shockley-Queisser limit. This is achieved using only the equivalence of about 10 nanometer composite material, comprising Ag and a thin film solar cell layer of a-Si, $CuInSe_2$ or the organic semiconductor MDMO-PPV. A potential for very resource efficient solar energy conversion based on plasmonics is thus demonstrated.

OCIS codes: (040.5350) Photovoltaic; (240.6680) Surface plasmons; (310.6628) Subwavelength structures, nanostructures

References and links

1. T. Markvart, and L. Castaner, eds. *Practical handbook of photovoltaics: fundamentals and applications* (Elsevier Advanced Technology, New York 2003).
2. H. J. Queisser, "Photovoltaic conversion at reduced dimensions," Physica E **14**, 1-10 (2002).
3. C. Hägglund, S. P. Apell, and B. Kasemo, "Maximized optical absorption in ultrathin films and its application to plasmon-based two-dimensional photovoltaics," Nano Lett., Article ASAP (DOI: 10.1021/nl101929j), http://pubs.acs.org/doi/abs/10.1021/nl101929j.
4. E. F. C. Driessen, F. R. Braakman, E. M. Reiger, S. N. Dorenbos, V. Zwiller, and M. J. A. de Dood, "Impedance model for the polarization-dependent optical absorption of superconducting single-photon detectors," European Physical Journal-Applied Physics **47**, 10701 (2009).
5. C. Hägglund, and B. Kasemo, "Nanoparticle plasmonics for 2D-photovoltaics: mechanisms, optimization, and limits," Opt. Express **17**, 11944-11957 (2009).
6. A. Alu, M. G. Silveirinha, A. Salandrino, and N. Engheta, "Epsilon-near-zero metamaterials and electromagnetic sources: Tailoring the radiation phase pattern," Phys. Rev. B **75** (2007).
7. H. A. Atwater, and A. Polman, "Plasmonics for improved photovoltaic devices," Nat Mater **9**, 205-213 (2010).
8. K. R. Catchpole, and A. Polman, "Plasmonic solar cells," Opt. Express **16**, 21793-21800 (2008).
9. H. A. Macleod, *Thin-film optical filters* (**Institute of Physics**, Bristol, 2001).
10. P. B. Johnson, and R. W. Christy, "Optical-constants of noble-metals," Phys. Rev. B **6**, 4370-4379 (1972).
11. M. I. Alonso, K. Wakita, J. Pascual, M. Garriga, and N. Yamamoto, "Optical functions and electronic structure of CuInSe2, CuGaSe2, CuInS2, and CuGaS2," Phys. Rev. B **63**, 075203 (2001).
12. H. Piller, "Amorphous Silicon," in *Handbook of Optical Constants of Solids*, E. D. Palik, ed. (Academic press, New York, 1985), p. 571.
13. H. Hoppe, N. S. Sariciftci, and D. Meissner, "Optical constants of conjugated polymer/fullerene based bulk-heterojunction organic solar cells," Mol. Cryst. Liquid Cryst. **385**, 233-239 (2002).

14. C. F. Bohren, and D. R. Huffman, *Absorption and Scattering of Light by Small Particles* (Wiley-VCH, Weinheim, 2004).
15. N. C. Lindquist, W. A. Luhman, S.-H. Oh, and R. J. Holmes, "Plasmonic nanocavity arrays for enhanced efficiency in organic photovoltaic cells," Appl. Phys. Lett. **93**, 123308-123303 (2008).
16. J. Le Perchec, Y. Desieres, and R. E. de Lamaestre, "Plasmon-based photosensors comprising a very thin semiconducting region," Appl. Phys. Lett. **94**, 181104-181103 (2009).
17. J. Vlieger, "Reflection and transmission of light by a square nonpolar llattice," Physica **64**, 63-81 (1973).
18. Y. S. Jung, "Spectroscopic ellipsometry studies on the optical constants of indium tin oxide films deposited under various sputtering conditions," Thin Solid Films **467**, 36-42 (2004).
19. M. W. Ribarsky, "Titanium Dioxide," in *Handbook of optical constants of solids*(Academic Press, 1985), pp. 795-804.
20. E. Moulin, P. Q. Luo, B. Pieters, J. Sukmanowski, J. Kirchhoff, W. Reetz, T. Muller, R. Carius, F. X. Royer, and H. Stiebig, "Photoresponse enhancement in the near infrared wavelength range of ultrathin amorphous silicon photosensitive devices by integration of silver nanoparticles," Appl. Phys. Lett. **95**, 033505 (2009).
21. NREL, "Reference Solar Spectral Irradiance: Air Mass 1.5," (American Society for Testing and Materials, 2003), http://rredc.nrel.gov/solar/standards/am1.5/ASTMG173/ASTMG173.html.
22. C. Hägglund, M. Zäch, G. Petersson, and B. Kasemo, "Electromagnetic coupling of light into a silicon solar cell by nanodisk plasmons," Appl. Phys. Lett. **92**, 053110 (2008).
23. J. H. Weaver, and H. P. R. Frederikse, "Optical properties of selected elements," in *CRC Handbook of Chemistry and Physics*, D. R. Lide, ed. (CRC Press, 2002).
24. W. Shockley, and H. J. Queisser, "Detailed balance limit of efficiency of p-n junction solar cells," J. Appl. Phys. **32**, 510-& (1961).
25. B. P. Rand, P. Peumans, and S. R. Forrest, "Long-range absorption enhancement in organic tandem thin-film solar cells containing silver nanoclusters," J. Appl. Phys. **96**, 7519-7526 (2004).
26. V. P. Drachev, U. K. Chettiar, A. V. Kildishev, H. K. Yuan, W. S. Cai, and V. M. Shalaev, "The Ag dielectric function in plasmonic metamaterials," Opt. Express **16**, 1186-1195 (2008).
27. J. R. Bolton, and M. D. Archer, "Requirements for ideal performance of photochemical and photovoltaic solar energy converters," J. Phys. Chem. **94**, 8028-8036 (1990).
28. C. Hägglund, M. Zäch, and B. Kasemo, "Enhanced charge carrier generation in dye sensitized solar cells by nanoparticle plasmons," Appl. Phys. Lett. **92**, 013113 (2008).
29. S. D. Standridge, G. C. Schatz, and J. T. Hupp, "Distance dependence of plasmon-enhanced photocurrent in dye-sensitized solar cells," J. Am. Chem. Soc. **131**, 8407-8409 (2009).
30. M. A. Green, K. Emery, Y. Hishikawa, and W. Warta, "Solar cell efficiency tables (Version 34)," Prog. Photovoltaics **17**, 320 (2009).
31. E. A. Coronado, and G. C. Schatz, "Surface plasmon broadening for arbitrary shape nanoparticles: A geometrical probability approach," J. Chem. Phys. **119**, 3926-3934 (2003).

1. Introduction

The layers responsible for light absorption in photovoltaic solar cells represent an important trade-off between the amount of material used and the amount of light absorbed. For instance, typical thin film solar cell materials require thicknesses in the range of 1 to 10 μm for sufficient light absorption.[1] If this thickness could be reduced without sacrificing absorption, manufacturing costs could be cut, resources and environment saved and the possible efficiency (that is, photovoltage[2]) increased. Based on the Thomas-Reiche-Kuhn sum rule, it can be estimated that the absorber layer thickness can be reduced to the nanoscale (~10 nm).[3] However, in such almost two-dimensional (2D) films, it turns out that the electrodynamic context (that is, the interactions between elementary dipole absorbers of the system) limits the absorptance to a maximum of approximately $n_i/(n_i + n_s)$ at normal incidence of light, where n_i and n_s are the refractive indices of the entrance and exit media surrounding the film, respectively.[3-5] In the symmetric case when $n_i = n_s$, at most 50% of the incident light is thus absorbed, with corresponding reflectance and transmittance of 25% each. To increase the absorptance towards 100%, one possibility is to use a metamaterial of very low effective permittivity[6] for the exit medium, such that $n_s << n_i$.

A conceptually and perhaps practically more simple approach to improve on the trade-off between reflectance and transmittance in 2D films, is to replace the exit medium with a dielectric spacer having a highly reflective backside, see Fig. 1. This reflective support (RS) does not only suppress transmittance of the incident radiation but may also help reduce the total reflectance of the system. Such anti-reflective behavior results from destructive interference between the fields reflected from the front and the back of the system,

respectively, and will here be shown to enable 100% absorptance in a 2D absorber film. We investigate and demonstrate this concept for practically feasible conditions, by considering ultrathin plasmonic core/shell nanoparticle arrays. Such systems may be geometrically designed to emulate the optimal conditions for absorption in 2D films, based on strong near-field coupling and efficient exchange of oscillator strength between its constituents.[3, 5] We find that the addition of an RS leads to results of very high interest for plasmonic solar cells[7-8] and other applications where extreme levels of absorption per unit volume is desirable. The paper is organized as follows:

In Sec. 2, we analyze a simple yet useful model for planar, ultrathin absorber layers supplemented by an ideal RS. We derive the optimal conditions at normal incidence of light, and show that in contrast to typical dielectric filters exploiting Fabry-Perot interference,[9] a very generous absorption bandwidth and angular response can be achieved in the optimized geometry. The center wavelength of the absorption band is given by the quarter-wave condition of the RS, while the angular response is largely decided by the critical angle defined between the entrance and spacer media surrounding the film.

In Sec. 3, the optimal conditions for absorption at a specific, target wavelength are implemented by means of plasmonic core/shell nanoparticle arrays. Using an effective medium representation of the array, the planar film model is applied to maximize the array absorptance at the target wavelength. Since the latter can be chosen differently from the characteristic center wavelength of the RS, not only the absorptance peak position but also the peak shape can be controlled. The results are compared to full 3D calculations by means of the finite element method (FEM).

In Sec. 4, the analytic model is finally applied to optimize the design of 2D plasmonic arrays towards broadband applications in solar cells. The resulting geometries are evaluated using FEM, assuming optically thick Al as the backside reflector. Absorber film nanocomposites of Ag[10] and the common but quite different thin film photovoltaic materials $CuInSe_2$,[11] amorphous silicon[12] and MDMO-PPV[13] are investigated.

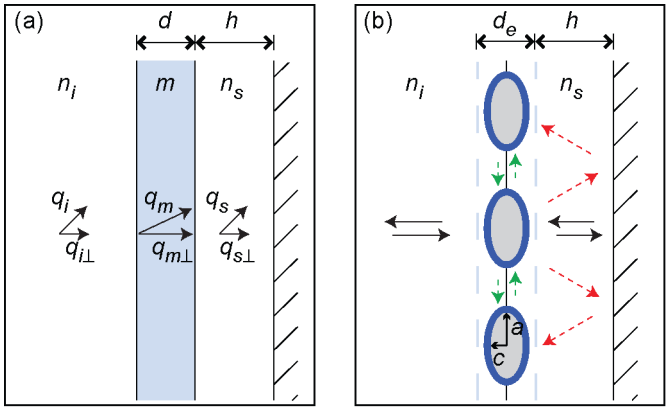

Fig. 1. Basic light absorbing structures under consideration. Light is assumed incident from the left in a dielectric medium of refractive index n_i. In (a), a light absorbing, planar thin film (complex refractive index m, thickness d) is supported by a dielectric spacer (refractive index n_s, thickness h) and an optically thick reflective substrate (to the right). In (b), the absorbing film is replaced by an array of identical, ellipsoidal shaped core/shell nanoparticles. The cores have a circular cross section of radius a in the array plane, and a semi-axis length c in the normal direction. The shells extend the core semi-axes by a fixed thickness. The array has an effective thickness d_e. Incident wave vectors and their normal components are represented by black arrows in (a), but it should be noted that their amplitudes are complex inside the film. In (b), the black arrows illustrate incident and specularly reflected fields for normal incidence of light. Scattered fields mediating lateral interactions between the particles in the array are shown as green, dashed arrows, while fields mediating interactions via the reflector are indicated by red, dashed arrows.

2. Maximized optical absorptance in ultrathin planar films with reflective support

Under the assumption of normal incident light from a medium of refractive index n_i, the planar film geometry described in Fig. 1a is first considered. An ultrathin absorbing film of thickness d and complex refractive index m is supported by a dielectric spacer layer of thickness h and refractive index n_s. An optically thick, highly reflective material is assumed at the back. We are interested in the situation when the thickness of the absorbing film is much smaller than the wavelength of light both outside (refractive indices ~1) and inside the film. Introducing the wavelength normalized absorber layer thickness as $\delta = 2\pi d/\lambda$, this means rigorously that $\delta << 1$ and $|m\delta| << 1$. To simplify modeling, we assume the reflector material at the back to be ideal (permittivity $\varepsilon \to -\infty$). The absorptance A associated with the absorber layer is then $A = 1 - |\tilde{r}|^2$, where $\tilde{r}$ is the total reflection coefficient of the system. The latter must take multiple reflections in all layers into account, and is found by solving the equations for the plane wave fields in each sub-layer of the structure with the appropriate boundary conditions.[14] This gives

$$\tilde{r} = \frac{r_i - r_d \gamma^2}{1 - r_i r_d \gamma^2}, \tag{1}$$

where for normal incidence of light, $r_i = (n_i - m)/(n_i + m)$, $r_d = (\tilde{n}_s - m)/(\tilde{n}_s + m)$ and $\gamma = \exp(im\delta)$. Defining λ_c as the wavelength fulfilling the quarter-wave condition of the dielectric spacer, that is, $\lambda_c = 4\, n_s h$, we further introduced $\tilde{n}_s = in_s \cot(\pi\lambda_c / 2\lambda)$. Eq. (1) has the same form as the expression for a thin film of complex refractive index m located between two media of refractive indices n_i and $\tilde{n}_s$, respectively.[3] At normal incidence, $\tilde{n}_s$ can therefore be interpreted as an effective refractive index of an optically thick medium representing the spacer layer plus the perfect reflector behind it. Since $\tilde{n}_s$ is purely imaginary, the normal component of the wave vector is imaginary and the fields exponentially decaying inside this 'RS'-medium; the transmittance is zero, as it should.

We assume that it is possible to tune the optical properties of the absorber layer, and investigate how the complex refractive index m should then be chosen to maximize its absorptance. Since there is no transmittance, a maximum is clearly the case if the total reflectance is completely suppressed. This can be achieved by requiring that $r_i = r_d \gamma^2$ in Eq. (1), which is mathematically similar to the ansatz previously used to identify the optimum for an ultrathin film without a reflector.[3] For small δ, the solution can thus be obtained by following the same procedure, resulting in an optimal complex refractive index given by

$$m^2 \approx i\frac{n_i - \tilde{n}_s}{\delta} = \frac{\lambda}{2\pi d}\left[in_i + n_s \cot\left(\frac{\pi\lambda_c}{2\lambda}\right)\right]. \tag{2}$$

This solution obviously satisfies $|m\delta| << 1$ as long as n_i and $\tilde{n}_s$ are finite. However, $\tilde{n}_s$ has poles at $\lambda = \lambda_c/(2N)$ for $N = 0, 1, 2\ldots$ This means, ultimately, that the absorption band including λ_c is defined by the semi-infinite wavelength interval $\lambda_c/2 < \lambda < \infty$ obtained for $N = 1$ and 0, respectively. In terms of photon energies $E \propto 1/\lambda$, the fulfillment of Eq. (2) would give 100% absorptance for $0 < E < 2E_c$, where $E_c \propto 1/\lambda_c$ defines the center energy of the band. It is also noteworthy that $\tilde{n}_s = 0$ when $\lambda = \lambda_c$, which leads to an optimum at $m = (1+i)(n_i/2\delta)^{1/2}$. The latter could have been obtained directly by consideration of a single thin film[3] between dielectric media of refractive index n_i and $n_s = 0$, respectively. Since n_i is assumed to be real and $\tilde{n}_s$ is imaginary, the magnitude of the optimal m is minimized in this quarter-wave situation, which can be understood as a consequence of constructive interference at the film position between incident and backside reflected fields. In contrast, if the spacer thickness is much reduced so that the ultrathin film is virtually located directly on the reflector

in a destructive interference node with vanishing electric field strength, the effective $|\tilde{n}_s| \to \infty$. This leads to diverging optimal optical constants of the film. In other words, the optimum of Eq. (2) cannot feasibly be fulfilled for absorber films placed directly on top of a reflector, which is a case previously addressed experimentally[15] and theoretically.[16]

The very broad absorption band derived with an RS stands in sharp contrast to typical thin film dielectric filters, whose bandwidths are limited by the refractive index contrast of the used thin film stack.[9] On the other hand, the results here require a wavelength dependence of the optical constants according to Eq. (2). We have further, implicitly, assumed an unlimited bandwidth of the perfect backside reflector. However, with highly reflective metals such as Al or Ag this need not impose serious limitations for visible to near-infrared light.

For photovoltaics and other applications, the dependence on the angle of incidence is also of high importance. With reference to Fig. 1a, this can be achieved by first using Snell's law to determine the normal components of the wave vectors in each layer. Eq. (1) can then be generalized to oblique incidence through use of $\gamma = \exp(iq_{m\perp}d)$ and the polarization dependent reflection coefficients. These are found as before, and are for TE-polarization,

$$r_i = \frac{q_{i\perp} - q_{m\perp}}{q_{i\perp} + q_{m\perp}} \text{ and } r_d = \frac{iq_{s\perp}\cot(q_{s\perp}h) - q_{m\perp}}{iq_{s\perp}\cot(q_{s\perp}h) + q_{m\perp}}, \tag{3}$$

and for TM-polarization

$$r_i = \frac{n_i^2 q_{m\perp} - m^2 q_{i\perp}}{n_i^2 q_{m\perp} + m^2 q_{i\perp}} \text{ and } r_d = \frac{in_s^2 q_{m\perp}\cot(q_{s\perp}h) - m^2 q_{s\perp}}{in_s^2 q_{m\perp}\cot(q_{s\perp}h) + m^2 q_{s\perp}}. \tag{4}$$

Using Eqs. (3)-(4), the absorptance of systems optimized for normal incidence according to Eq. (2) can be evaluated for oblique incidence. Typical results are shown in Fig. 2. A characteristic increase of the reflectance, and hence loss of absorptance, is observed for TM-polarization near the critical angle, arcsin(n_s / n_i), formed between the media surrounding the film. It is favorable to have a high magnitude of this generally complex angle. This is achieved for $n_s > n_i$ and results in a diminished role of the spacer thickness (λ_c). For instance, with $n_s = 2$ and $n_i = 1.5$, the polarization-averaged absorptance exceeds 90% for angles up to 53° (Fig. 2c, both cases).

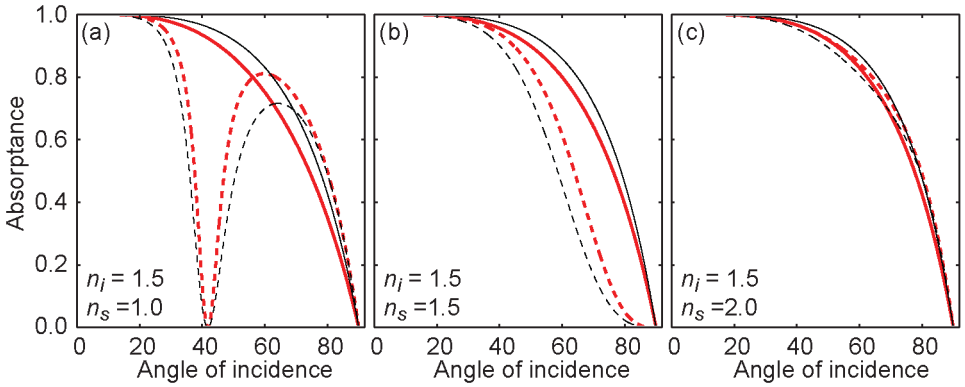

Fig. 2. Angular responses for practically 2D thin films ($\delta \sim 10^{-4}$), maximizing the absorptance at normal incidence of TE- (solid lines) and TM-polarized light (dashed lines). The incident wavelength was $\lambda = 840$ nm and $n_i = 1.5$. The center wavelength was either $\lambda_c = \lambda = 840$ nm (red, thick lines) or $\lambda_c = 550$ nm (black, thin lines). The refractive index of the spacer layer was in (a) $n_s = 1$; in (b) $n_s = 1.5$ and in (c), $n_s = 2$. The dip in the TM-polarized case is at the critical angle between the external media, here occurring at 42, 90 and 90-46i° (complex angle), respectively. The influence of λ_c (and thus spacer thickness) is less dramatic.

3. Realization of optimal conditions in nanoparticle arrays with reflective support

The previous analysis reveals that, under close to ideal conditions, an absorptance exceeding 90% can be achieved in virtually 2D absorber layers, over a very broad band of wavelengths and angles of incidence. Unfortunately, homogenous absorber materials typically do not fulfill the requirements of Eq. (2) over the spectral range of relevance for many practical applications, including photovoltaics. On the other hand, it was recently shown feasible to realize similar conditions at a targeted wavelength by means of arrays of plasmonic core/shell nanoparticles, or plasmonic nanoparticles located on top of an ultrathin, continuous semiconductor layer.[3, 5] Such nanocomposites behave much as truly two dimensional, homogeneous layers from an optical viewpoint.[3] We will therefore investigate if the optimum with a reflective support is approachable by means of ultrathin nanocomposites of plasmonic metals (Ag) and semiconductor materials used for thin film photovoltaics.

To this end, we consider a particle array represented as a planar, homogeneous, effective medium thin film,[3] and use the expressions derived for planar films to evaluate the response in presence of the RS. This approach neglects particle-particle interactions mediated by field components that have been scattered off the incident light propagation direction and subsequently reflected at the back, see further the red, dashed arrows in Fig. 1b. On the other hand, it does take the more important self-image interactions into account (black arrows in Fig. 1b), as well as direct particle-particle interactions in the array (dashed green arrows in Fig. 1b), to lowest orders in the wavelength normalized lattice constants.[3] The model is expected to give accurate results when the dimensions of the particles and the array are much smaller than the incident wavelength, and sufficiently small compared to the spacer layer thickness.

More specifically, we assume a square array with lattice constant Λ, situated in a homogeneous external medium so that in terms of Fig. 1b, $n_i = n_s \equiv n_e$. The effective complex refractive index of the array at normal incidence is then approximated by[3, 17]

$$m_e^{\,2} = \frac{2 n_e F \overline{\alpha}}{\delta_e \left(1 - f \overline{\alpha}\right)}, \tag{5}$$

where $\delta_e = 2\pi d_e / \lambda$, and d_e is the effective film thickness, see Fig. 1b. For a consistent treatment of the problem, properties such as reflectance and absorptance must be evaluated for an effective array thickness in the 2D limit, that is $d_e \to 0$.[3] The parameter $f = 1.08 V / \Lambda^3$ is here a volume filling factor with V being the total particle volume, while $F = 3\pi n_e V / (\lambda \Lambda^2)$ is a surface measure. Further, $\overline{\alpha}$ is the single particle polarizability[14] normalized by $3V/(4\pi)$. In order to realize complete absorption in the array, the effective medium refractive index of Eq. (5) must fulfill Eq. (2). This leads to the condition

$$\left[f - \frac{2 i n_e}{n_e - \tilde{n}_s} F \right] \overline{\alpha} = 1. \tag{6}$$

Eq. (6) can be used to determine the geometry such that the model absorptance is 100% at a target peak wavelength λ_0. Note that this wavelength may be chosen differently from the center wavelength λ_c associated with the RS alone. The spectral distribution of the absorptance is finally obtained from $A = 1 - |\tilde{r}|^2$, where the reflection coefficient $\tilde{r}$ is obtained from Eq. (1) with $m \to m_e$ from Eq.(5). For numerical purposes, d_e is set to a small finite value, such that the result does not depend on its variation.

Comparison of the analytical results of this model and full three dimensional finite element solutions for the same core/shell particle systems has been performed for a range of parameter values and materials, see Fig. 3 for an example with $CuInSe_2$[11] in the shells and Ag[10] in the cores. In this example, an external medium refractive index $n_e = 2$ is assumed,

which is reasonably representative for transparent conductive media such as ITO[18] and wide bandgap semiconductors such as TiO_2.[19] The idea is that layers of such materials could provide a conduction path to the front and back electrodes in a solar cell configuration resembling the one recently investigated experimentally by Moulin et al.[20] We have not included losses in these layers, however, since we are interested primarily in an ideal situation where those would be negligible. The model is able to reproduce the main features and behavior of the FEM solutions, as long as the dimensions in the system, especially the particle size along the incident light propagation direction, are small compared to the wavelength. From Eq. (2), we saw that if the spacer thickness is chosen to fulfill the quarter-wave condition at the target wavelength, such that $\lambda_c = \lambda_0$, a minimum magnitude of the optimal m_e results. This generally translates to a minimum amount of material in the optimized array, and a quite symmetric shape about the peak maximum. An offset of λ_c from the maximum at λ_0 mainly results in a shift of the peak weight towards λ_c.

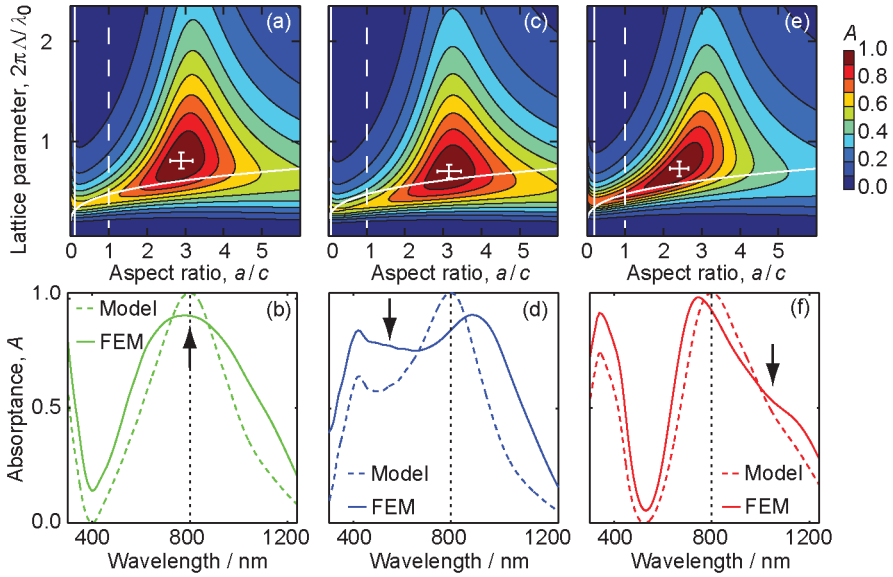

Fig. 3. (a) Model absorptance in a square Ag-core/$CuInSe_2$-shell nanoparticle array, as a function of the normalized lattice constant Λ and the aspect ratio *a*/*c* of the cores. The target wavelength was $\lambda_0 = 800$ nm and the external medium refractive index $n_e = 2$. The volume equivalent radii of the particle cores were 20 nm, the shell thicknesses 10 nm and the spacer thickness such that the center wavelength was $\lambda_c = 800$ nm. For very small aspect ratios, the requirement that the particles do not touch the back reflector limits the parameter space. The further condition that they should not touch each other bounds the parameter space from below. These limits are indicated by solid white lines to the far left and below the maxima. The vertical, dashed white line distinguish prolate (left) and oblate (right) particle shapes. Maximum absorptance of 100% is predicted at the white cross. The cross size represents ±10% changes of the underlying variables, and ends above the 90% absorptance contour. This indicates a relatively high robustness of the optimum in this parameter space. In (b), the absorptance for the geometrical conditions at the cross in (a) are shown as a function of incident light wavelength. The model calculation is compared to calculations by FEM for the same set of parameters, including an ideal backside reflector. The black arrow indicates λ_c and the vertical line λ_0. In (c) and (d), the same conditions applies, except that the center wavelength λ_c of the support is offset to 550 nm. In (e) and (f), λ_c is offset to 1050 nm instead. The main effect of these offsets is a skewing of the absorptance peak shape about the maximum.

4. Optimization of 2D plasmonic solar cells

The results of the model are sufficiently accurate to provide useful orientation in the complex parameter space encountered when optimizing these type of nanocomposite systems for plasmonic solar cells. For this purpose, we distinguish between absorption in the metal and semiconductor parts of the array. It is assumed that absorption in the metal parts is entirely lost to heat dissipation, which is often but not necessarily the case.[20] It is further assumed that the absorption in the semiconductor part, A_{pv}, results in useful charge carriers with unit quantum efficiency. In this case, it has previously been argued that the plasmon induced absorptance, $\Delta A \equiv A_{pv} - A_{ref}$, is an appropriate figure of merit to quantify the benefit of having the plasmonic particles in the system.[5] A_{ref} is here a reference absorptance, representative of a similar system but which lacks the plasmonic components. For simplicity, we consider a planar film of the shell semiconductor material as a reference absorber layer, just as in the situation described in Fig. 1a. The reference film thickness (d in Fig. 1a) is taken as the equivalent thickness of the array, calculated as the total volume of metal and semiconductor material per unit area. With the intention to optimize the plasmonic structure with regards to the total response at normal incidence of sunlight, the plasmon induced absorptance is integrated up to the threshold wavelength defined by the bandgap of the material, λ_G. In this integration, the AM1.5G solar spectral photon flux density[21] $N(\lambda)$ is taken into account through a weighting by the normalized distribution $w(\lambda) \equiv N(\lambda) \Big/ \int_0^{\lambda_G} N(\lambda')\, d\lambda'$. The angular distribution of sunlight due to haze is not taken into account here, but on the other hand, a good response at oblique angles is feasible in the long wavelength limit if judging from the planar film results of Fig. 3. In brief, the system is thus maximized with respect to the spectrally weighted plasmon induced semiconductor absorptance,

$$\Phi = \int_0^{\lambda_G} w(\lambda)\, \Delta A(\lambda)\, d\lambda \,. \tag{7}$$

This figure of merit is a measure of the 'useful' absorptance added to the system through the presence of the plasmonic particles. In principle it has a maximum of $\Phi = 1$, but this is not realistic considering the simultaneous requirements to absorb all incident photons up to λ_G in the semiconductor part of the array alone, while nothing is absorbed in the reference film.[5]

To obtain an analytic estimate for Φ, the proportions absorbed in the metal and semiconductor parts, respectively, are needed. Based on the fundamental relation that the local absorption rate is for non-magnetic media directly proportional to the damping part of the permittivity, these branching ratios can be estimated at the peak wavelength λ_0, as was recently shown.[3] Briefly, the geometry is optimized and the damping of the semiconductor (as expressed by the imaginary part of its permittivity, Im ε_{sc}) is compared to the damping of an artificial material with a permittivity $\varepsilon_{sc}^{\,0}$. The latter permittivity is chosen to maximize the absorptance in the same geometry when the damping in the metal part of the structure is suppressed (Im $\varepsilon_{met} \to 0$). The resulting estimate for the semiconductor absorptance is

$$A_{sc}(\lambda_0) = \Gamma_0 A(\lambda_0) \,, \tag{8}$$

where $A(\lambda_0)$ is the total absorptance at the peak (that is, 100%), and the branching ratio for semiconductor absorptance is obtained from $\Gamma_0 = \text{Im}\, \varepsilon_{sc} / \text{Im}\, \varepsilon_{sc}^{\,0}$. To keep things simple in the optimization, Γ_0 is assumed representative for the average branching ratios across the relevant wavelength interval. In the end, a more accurate value of Φ is then obtained by use of the identified parameter set in a full, 3D FEM calculation of $A(\lambda)$ and the actual, wavelength dependent branching ratio $\Gamma(\lambda)$. Details regarding FEM calculations are presented elsewhere.[5, 22] To make the FEM evaluation more practically relevant, the perfect reflector

boundary condition used in the analytic model is replaced by an impedance boundary condition simulating an optically thick Al metal film.[23]

We connect the results further to photovoltaic solar cells by relating them to the Shockley-Queisser efficiency limit η_{SQ}.[24] This is an estimate of the ideal efficiency of a single junction solar cell having a particular semiconductor bandgap. It assumes that all incident photons of energies exceeding the bandgap are absorbed and contribute equally to the solar cell output. The spectrally weighted average absorptance in the semiconductor,

$$\langle A_{sc} \rangle = \int_0^{\lambda_G} w(\lambda) A_{sc}(\lambda) d\lambda \,, \tag{9}$$

is therefore an estimate for the fraction of the SQ efficiency limit that could, ideally, be realized unless metal absorption could also be exploited. From this, the corresponding conversion efficiency is $\eta = \langle A_{sc} \rangle \, \eta_{SQ}(\lambda_G)$.

Even with analytic approximations at hand, a maximization of Eq. (7) is a quite formidable task. For the core/shell system described in Fig. 1b with fixed homogeneous external media of refractive index n_e, there are still five independent parameters to determine. These may be represented as the particle shell thickness, core aspect ratio a/c, core volume [or the equivalent sphere radius $r_o \equiv (a^2 c)^{1/3}$], lattice constant Λ and RS center wavelength λ_c. To deal with this parameter space, the analysis is restricted by two conditions. The first is that the total absorptance is 100% at some, optimized, wavelength λ_0. Although this condition should yield solutions close to the true optimum when metal dissipation is small, the integrated response could in principle be improved by relaxing it. After all, it is the semiconductor absorptance rather than the total absorptance which should be high. On the other hand, when the former is already close to maximum (that is, ~ 90% of the total), there cannot be a dramatic improvement. A second limitation is that we focus on solutions for which $\lambda_c = \lambda_0$. This usually approximates a local maximum in the figure of merit, but from other viewpoints it could be advantageous to 'tweak' the response as shown in Fig. 3, and obtain a better spectral coverage.

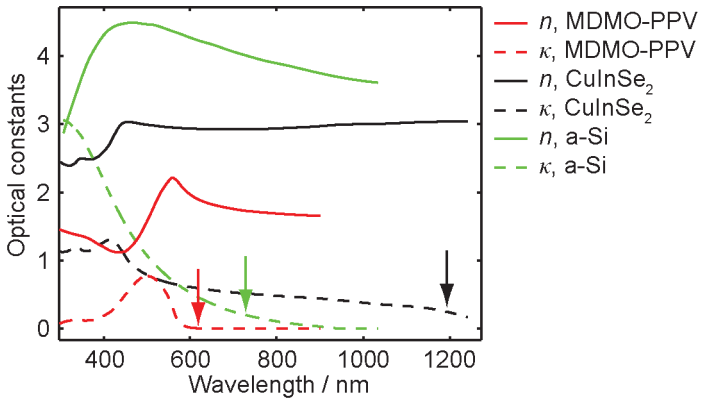

Fig. 4. Optical constants of thin film solar cell materials considered. The approximate positions of the bandgap thresholds are indicated by the arrows.

To illustrate our optimization approach and the high potential and versatility of these type of solar cell configurations, we consider core/shell nanoparticle arrays with Ag particle cores. The optical constants used for Ag[10] represent high quality films with relatively low damping, but have been proven useful under relevant experimental conditions.[25-26] We do not include damping due to surface scattering in the Ag permittivity at this point, but discuss its implications in Sec. 4.

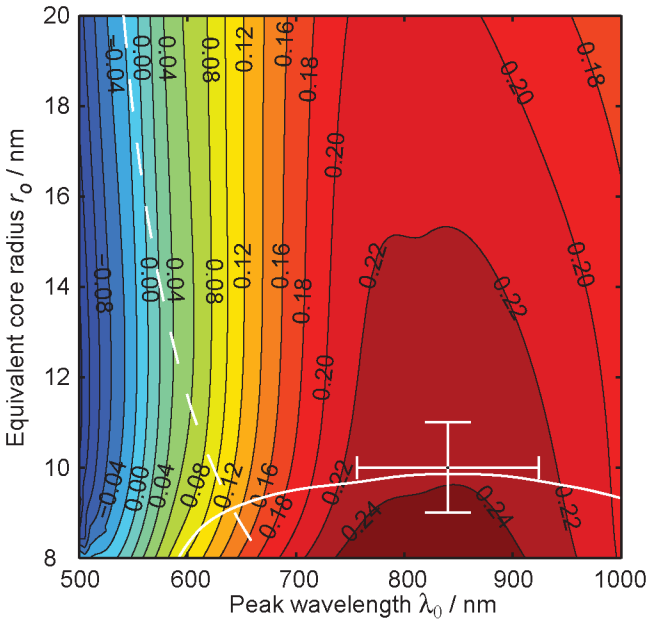

Fig. 5. Spectrally weighted plasmon induced absorptance [Φ, see Eq. (7)] as a function of the equivalent sphere radius of the core and the peak wavelength λ_0. In this map, the particle aspect ratios and the lattice constants were optimized to maximize the total absorptance for each value of r_o and λ_0. The particle cores are assumed to be Ag, and the shells are $CuInSe_2$ with a fixed thickness of 5 nm. The external medium refractive index is $n_e = 2$. Particles are prolate to the left of the white dashed curve, and oblate to the right. Unphysical overlap of the particles occurs below the solid white line, which leads to an approximate position of the valid local maximum at the cross mark. At this point, the core aspect ratio is $a/c \approx 2.7$ and the lattice constant $\Lambda \approx 38$ nm. The cross arms have lengths corresponding to 10% of the underlying parameters, and show that the optimum is relatively robust to deviations also for these parameters.

The shells are either taken to be $CuInSe_2$,[11] a-Si,[12] or the organic semiconductor MDMO-PPV.[13] These semiconductors are commonly employed in thin film photovoltaics and are all heavily damped with $\mathrm{Im}\,\varepsilon = 2n\kappa \sim 1$ in relevant parts of the spectrum. However, their optical constants and bandgaps differ significantly, as shown in Fig. 4.

For the practical optimization procedure, maps of the type illustrated in Fig. 5 are generated for the figure of merit Φ, as a function of particle core volume (r_o) and target peak wavelength (λ_0). Each map is achieved for a trial shell thickness by numerical determination of the combination of a/c and Λ which maximizes the total absorptance (as in Fig. 3), at each point (r_o, λ_0). The resulting geometry is taken as an input for calculating the integrated figure of merit according to Eq. (7), which is presented in the map. The map is then used to identify the best solution subject to the constraints that the particles do not overlap each other nor the reflective backside of the support. Also, only solutions compatible with the long wavelength limit should be considered. The whole procedure is iterated to determine an appropriate shell thickness. The results are presented in Table 1 and Fig. 6.

In the first example, presented in Fig. 6a, the Ag-core/$CuInSe_2$-shell system mapped in Fig. 5 is considered. The optimized geometry results in a FEM calculated plasmon induced absorptance of $\Phi = 33\%$, but the spectral response shows that the absorptance in the region between 400 and 700 nm is relatively weak.

Table 1. Conditions and results for optimized Ag-core/semiconductor-shell nanoparticle arrays

Shell material	Optimized parameters					Other characteristics				FEM Results		
	λ_0	Λ	a	c	d_{sc}[a]	λ_c	t_{Ag}[b]	t_{sc}[c]	η_{SQ} / % [27]	Φ, Eq. (7)	$\langle A_{sc} \rangle$, Eq. (9)	η / %
$CuInSe_2$[11]	840	38	14	5.1	5.0	840	2.8	7.5	31	0.33	0.55	17
$CuInSe_2$[11]	840	42	15	6.5	5.0	550	3.6	7.7	31	0.31	0.66	20
a-Si[12]	625	66	13	29	10	625	4.7	15	29	0.28	0.64	18
MDMO-PPV[13]	535	43	13	10	2.0	535	3.9	2.3	21	0.38	0.54	12

All lengths are in nm units.
[a]Semiconductor shell thickness.
[b]Equivalent thickness of Ag (core).
[c]Equivalent thickness of semiconductor (shell).

By introducing an offset between the two characteristic wavelengths, such that $\lambda_c = 550$ nm and $\lambda_0 = 840$ nm, a better coverage of the solar spectrum can be achieved, see Fig. 6b. The result is a slight reduction of the figure of merit, but also an increase of $\langle A_{sc} \rangle$ from 55 to 66%. The latter corresponds to a 20% ideal conversion efficiency based on the $CuInSe_2$ bandgap of 1.04 eV.[27] The total equivalent thickness of the particle array increases from 10 to 11 nm, which is nevertheless a remarkably small amount of material in this context.

Another example is the Ag-core/a-Si-shell system, shown in Fig. 6c. For this case, prolate particles are found to be optimal, leading to an average absorptance $\langle A_{sc} \rangle = 64\%$. In terms of an ideal conversion efficiency based on a bandgap of 1.7 eV, this corresponds to 18%. The total equivalent thickness is again very small, about 20 nm.

As a final example, we consider the Ag-core/MDMO-PPV-shell system, with an optimized response shown in Fig. 6d. Here, $\langle A_{sc} \rangle = 54\%$ results in an ideal efficiency of 12% for a bandgap of 2 eV. The equivalent absorber layer thickness is only 6.1 nm. The 2 nm shell thickness identified approaches that of a monomolecular layer of the organic semiconductor, and it is questionable how relevant the bulk properties shown in Fig. 4 are. The results nevertheless give a rough idea of what can be achieved for these type of systems, which also include dye-sensitized devices.[28-29]

In general, it is clear that the analytic model agrees sufficiently well with the full FEM calculations to be of use for this kind of optimization. Some deviations results from the difference between Al and the perfect reflector assumed in the model. These deviations can be appreciated from a comparison of the analytic and FEM reference systems in Fig. 6, since the analytic solution is exact for this case. Additional deviations in the particle systems stem from the neglect of interparticle-couplings mediated by the reflector, and of higher order particle modes influencing at short wavelengths. The latter may explain the very strong response in the near-UV range for the prolate particles in the a-Si system, see Fig. 6c. The fact that the particles are in this case relatively extended in the normal direction leads to field retardation and stronger coupling to quadrupolar resonances. When it comes to the estimate for branching ratio for semiconductor absorptance at the peak wavelength, it is usually in good agreement with the FEM results, although the absolute absorptance values differ somewhat. Compared to its value at the absorption peak, the branching ratio is typically higher for shorter wavelengths. This may partially be accounted for by higher semiconductor damping in this region. Closer to the bandgap threshold, the semiconductor damping is weaker and the branching ratio decreases. The influence of higher order modes at short wavelengths, with their radial field energy distribution more concentrated towards the metal/semiconductor interface,[14] could possibly also contribute to this trend.

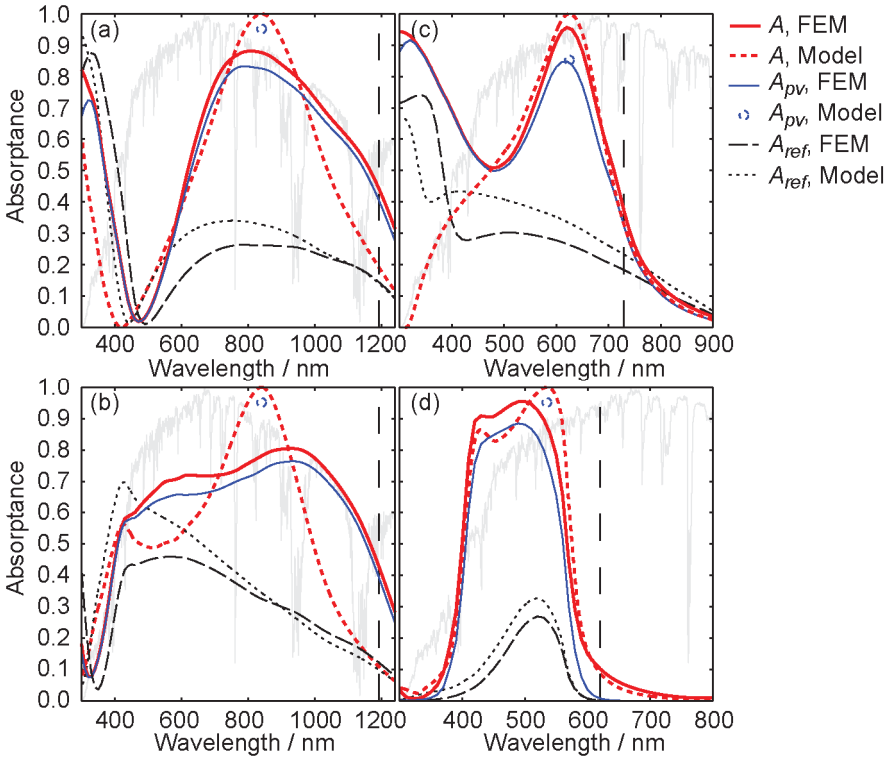

Fig. 6. Analytic model and FEM calculated absorptance for core/shell systems selected on merits of their high spectrally weighted plasmon induced absorptance. The spectral photon flux distribution of AM1.5G sunlight (light grey, in arbitrary units) is included for comparison. The particle cores consist of Ag and the shells of different solar cell materials. Identical systems are considered in the different types of calculations, except that a more realistic Al backside reflector is simulated in the FEM calculations instead of the perfect reflector assumed in the model. In (a) and (b), the PV shells consist of $CuInSe_2$, with the difference that the RS center wavelength is chosen equal to the peak wavelength at 840 nm in (a), and to 550 nm in (b), respectively. In (c), the shell material is a-Si, and in (d), it is the organic semiconductor MDMO-PPV. The circular symbols show estimates for the shell absorption at maximum, based on the analytic model.

5. Discussion

Several assumptions were made to arrive at an analytic model and a broadband integrated figure of merit for plasmonic solar cells based on ultrathin (2D) absorber layers and a reflective support.

The model approximations were:

- A perfect backside reflector.
- Long wavelength limit for the particles and their lateral interactions.
- No reflector mediated interparticle-couplings.

The model optimization assumed:

- That the analytic estimate of the branching ratio for semiconductor absorption at the peak wavelength λ_0 is representative for the whole spectral range of importance.
- That the requirement for a total absorptance of 100% at some λ_0 does not cause a strong deviation from the optimal solution.
- A fixed external medium refractive index of $n_e = 2$.
- Spacer thicknesses approximately fulfilling the quarter-wave condition $\lambda_c = \lambda_0$.

Finally, the figure of merit and efficiency evaluations by FEM assumed:

- 100% internal quantum efficiency in semiconductor parts and 0% in metal parts.
- Optically loss-free entrance and spacer media.
- Normal incidence of light.

It is important to note that the model served only as a guide to optimal conditions, which were in the end evaluated using FEM. The approximations of the model causes deviations from the optimum of the FEM calculation, and therefore always have a more or less negative influence on the achieved values. Likewise, the assumptions and constraints in the optimization to some extent lowers the figure of merit and the conversion efficiency found by FEM. Especially, gains could be made by requiring the shell absorptance rather than the total absorptance to be maximized at a particular wavelength, or by omitting such constraints completely. This aspect becomes more important in cases where dissipation losses in the metal part are significant.

What remains are the assumptions regarding optically loss-free external media, internal quantum efficiencies and the neglect of angular dependence in the integrations. They lead to an overestimate of the realistically obtainable efficiency, but are often made for these type of estimates.[24, 27] They may be justified for an ideal case. For instance, wide bandgap semiconductors could in principle function as electron or hole acceptors and would not necessarily cause much parasitic absorption in the system. Likewise, the internal quantum efficiencies could ideally approach 100%, as they do in well functioning solar cells. The situation at hand, with metal/semiconductor nanocomposites, is largely unexplored in this respect, making it difficult to take into account in the model. Finally, the effect of oblique angles of incidence are not expected to be dramatic, since an attractive angular dependence (that is, $> 90\%$ of the peak value up to $\approx 50°$ angle of incidence) was found for the planar system under feasible conditions. It can be argued that the response of the array will be qualitatively similar in the long wavelength limit, with the main difference being that the effective properties are anisotropic because of the, generally, anisotropic polarizabilities of the particles.[14] This view is in line with the measured angular dependence of a related system.[22]

With these shortcomings in mind, the results connected to Fig. 6 can be taken as rough estimates for what can be achieved in practice. They represent a very promising reduction of the amount of material used in today's thin film solar cells by typically a factor 100, while the estimated ideal efficiencies are reduced by less than a factor 2. These efficiencies are in fact still higher than the record efficiencies for devices based on much thicker layers of similar materials.[30] The very much thinner active layers suggested here further provide many new opportunities to bring the systems closer to their ideal conversion efficiencies, especially since the charge carrier conduction paths will be correspondingly shorter. As exemplified in Figs. 3 and 5, a relatively high robustness to geometric perturbations results as a consequence of the strong coupling to a heavily damped semiconductor material. Finally, there is a good chance to increase the efficiency further without much additional resources, since the model analysis was restricted to truly ultrathin ($\delta << 1$ and $|m\delta| << 1$) films here. If going beyond this 2D limit, internal Fabry-Perot interference in the absorber film, corresponding to collective multipolar modes in the particle arrays, will develop. These modes can provide additional width to the spectral response and thereby contribute to yet higher conversion efficiencies. Whether they may also allow for higher figure of merits for the benefit of plasmonic particles in solar cells, is left as an open question.

From a practical viewpoint, one challenge lies in achieving sufficient quality of the interfaces between the semiconductor and plasmonic parts of the absorber structure. These interfaces are critical for a strong near-field coupling and exchange of oscillator strength, and thereby for the achievable peak widths, branching ratios and robustness of the system. Another concern is to what extent the relatively low damping of the Ag nanoparticle cores used in the presented calculations can be approached in practice. Defects, grain boundaries and impurities would increase this damping, as would surface scattering effects for core sizes

smaller than the electron mean free path (about 50 nm for Ag). Although it is not obvious that inelastic surface scattering would exclusively be associated with useless dissipation in this context, this process could potentially increase the metal damping by up to roughly a factor two compared to the bulk value of Ag for the optimized core sizes presented in Table I.[31] From the discussion around Eq. (8), proportionally higher dissipation losses in the metal part of the structure would then be expected. This does not alter our main conclusions, however, since the losses would increase from a relatively modest level compared to the semiconductor absorptance (Fig. 6), and since they could be reduced through the use of larger particles, which does not diminish the figure of merit much (see Fig. 5). A less constrained optimization would help defeat such losses further.

6. Conclusions

Plasmonic solar cells based on virtually 2D absorber films supplemented by a non-absorbing spacer and a highly reflective backside constitute very interesting options for resource efficient solar energy conversion. We developed a simple analytic model for absorber layers of plasmonic core/shell nanoparticle arrays, applicable in the long wavelength limit. The model agrees well with finite element calculations and allows for understanding and design of the spectral and angular responses of these type of systems. It also allows for optimization towards broadband solar energy applications. Based on common thin film solar cell materials and Ag, we found that maximization of the spectrally integrated plasmon induced absorptance in the semiconductor part leads to configurations of equivalent active layer thicknesses of only around 10 nm, with ideal solar energy conversion efficiencies of up to 20%.

Acknowledgements

CH acknowledges funding from FP7 (‘PRIMA’, STREP-248154) and from the Swedish Energy Agency (‘Nano-SEE’, 181-1). SPA is grateful for funding from the Swedish Foundation for Strategic Research (‘Functional Electromagnetic Metamaterials’, RMA 08-0109).